Supporting Information

$Al_{12}Co_4$: A Pioneering Heterometallic Aluminum-Oxo Cluster with Exposed Co Sites for Oxygen Evolution Reaction

Er-Meng Han,[a‡] Ru-Xin Meng,[a‡] Yi-Qi Tian,[a] Jun Yan,[a] Kai-Yu Liu,[a*] Chao Liu[*]

College of Chemistry and Chemical Engineering, Central South University, Changsha 410083, Hunan, P. R. China

1. Experimental section

Materials and Characterization. All reagents were purchased commercially and were not further purified when used. Powder X-ray diffraction (PXRD) analysis were performed on a Rigaku Mini Flex II diffractometer at a 2θ range of 3–50° (5° min^{-1}) with CuKα radiation (λ =1.54056 Å). The solid-state UV/Vis spectra data of the cluster samples were obtained on UV-4000 spectrophotometer. Electrospray ionization mass spectrometry (ESI-MS) were performed on a Bruker Daltonik GmbH (Bruker, Germany). Thermogravimetric (TGA) patterns were recorded on a Mettler Toledo TGA/SDTA 851e analyzer in a N_2 atmosphere. FT-IR spectra using KBr pellets were taken on a Bruker Vertex 70 Spectrometer.

Synthesis for the cluster $\{Al_{12}Co_4O_8(OH)_{10}(TBC[4])_4(DMF)_8Cl_2\}\cdot 18DMF$ $\{Al_{12}Co_4\}$: For the preparation of **$Al_{12}Co_4$** clusters, TBC[4] (17 mg, 0.026 mmol), cobalt chloride (30 mg, 0.23 mmol), and 3 mL DMF were combined in a 10 mL glass bottle. To this mixture, $Al(O^iPr)_3$ (30 mg, 0.15 mmol) was added. The solution underwent sonication for 15 minutes and was subsequently placed in an oven at 100℃ for a period of 3 days. Lavender-hued crystals of **$Al_{12}Co_4$** were obtained, followed by washing with DMF, and finally, air-drying at room temperature. The yield of the procedure was approximately 28%.

Synthesis for the cluster $\{Al_6O_2(OH)_6(H_4TBC[8])_2(DMF)_4\}\cdot 12DMF$ $\{Al_6\}$: TBC[8] (30 mg, 0.046 mmol), and 3 mL DMF were added into a 10 mL glass bottle, and then added with $Al(O^iPr)_3$ (20mg, 0.1 mmol). The solution was sonicated for 15 min, then transferred.to an oven at 80℃for 3 days. Thin, colorless crystals of **Al_6** were obtained and washed with DMF, then dried at room temperature (yield: ~50%).

X-ray crystal structure determination. Single crystal diffraction data was collected on Bruker D8 Venture diffractometer with liquid metal Ga Kα radiation. The structures were solved using intrinsic phasing methods in ShelXT program and then refined by full-matrix least-squares on F^2 using ShelXL-2014 in Olex[2] program. The hydrogen atoms were introduced at their geometric positions and refined as riding atom, and the positions of non-hydrogen atoms were refined with anisotropic displacement parameters during the final cycles. Due to the rotation disorder of tert-butyl groups, in all cases the ISOR, DELU and SIMU constraints were necessary to achieve convergence. The SQUEEZE operation was used to eliminate the contribution of disordered solvent molecule to the reflection intensity. For **Al_6**, the crystals are thin and small in size, and they tend to stack together, making it challenging to select a high-quality crystal for testing. Consequently, the resulting diffraction data exhibits a relatively high R_{int} value (22.99%). However, despite these challenges, the analyzed crystal structure is remarkably clear, as evidenced by a low R_1 value of only 10.73%. A summary of the crystallographic data for the reported clusters is listed in Table S1. CCDC 2272820 and 2283848 contain the crystallographic data herein.

Electrodes preparation. The catalyst ink was prepared by dispersing 1 mg **$Al_{12}Co_4$** cluster, 9 mg CNTs, and 20 μL Nafion solution (5 wt%) in a mixture of 1 mL ethanol solution by sonication for 30 min to form a homogeneous ink. Then 50 μL of the homogeneous ink was loaded onto the two sides of a carbon fiber paper electrode with 1×1 cm^2, which was air-dried overnight before used.

Electrochemical measurements. All the electrochemical experiments were carried out in a three-electrode system in 1 M KOH electrolyte, with the as-prepared samples on carbon cloth as the working electrode, a graphite rod as the counter electrode and an Hg/HgO electrode as the reference electrode. Linear sweep voltammetry (LSV) was analyzed with a scan rate of 10 mV s^{-1}. All potentials were calibrated by the Nernst equation: $E_{RHE}=E_{Hg/HgO}+0.0592\times pH+0.098$, $\eta = E_{RHE} - 1.23$ V, where η is the overpotential. In addition, the Tafel slope was modeled by Tafel equation: $\eta = b\log j + a$, where g is the overpotential, b is the Tafel slope, j

is the current density and a is a constant. Chronoamperometry measurements were tested at a static potential, and the electrochemical impedance spectroscopy (EIS) was performed in the frequency range from 10 kHz to 10 mHz with an amplitude of 10 mV. The generated gases were measured by GC-2014C gas chromatograph (Shimadzu, Japan).

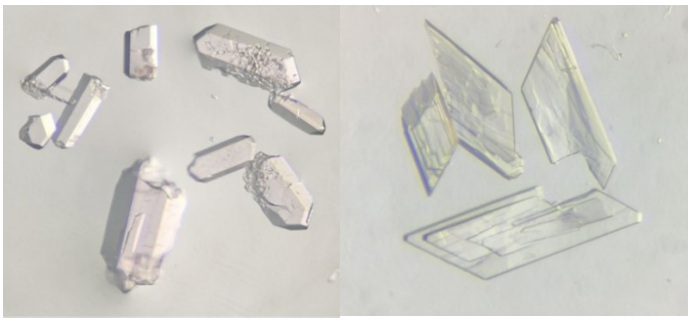

Figure S1. Picture of crystals of $\mathbf{Al_{12}Co_4}$ (left) and $\mathbf{Al_6}$ (right).

1. Structure of Compounds

Table S1. X-ray measurements and structure solution of compounds.

Compounds	**$Al_{12}Co_4$**	**Al_6**
CCDC	2272820	2283848
Formula	$C_{254}H_{400}Al_{12}Cl_2Co_4N_{26}O_{60}$	$C_{224}H_{330}Al_6N_{16}O_{40}$
F_w	5408.43	4048.90
Crystal system	monoclinic	triclinic
Space group	*C2/c*	P-1
a, Å	38.1054(16)	16.830(2)
b, Å	23.6556(11)	18.597(3)
c, Å	34.533(2)	20.790(3)
α/°	90	110.867(7)
β/°	113.372(2)	111.132(6)
γ/°	90	93.254(7)
V, Å^3	28574(3)	5542.1(13)
Z	4	1
ρ_{calcd}(gcm^{-3})	1.187	0.950
μ (mm^{-1})	1.980	0.459
F(000)	10856.0	1704.0
Data/restraints/parameters	29060/78/1568	20100/117/1055
Goof	1.000	0.895
R_1/wR_2(I> 2σ(I))	0.0749/0.1917	0.1073/0.2434
R_1/wR_2(all data)	0.1290/ 0.2230	0.2902/0.3273

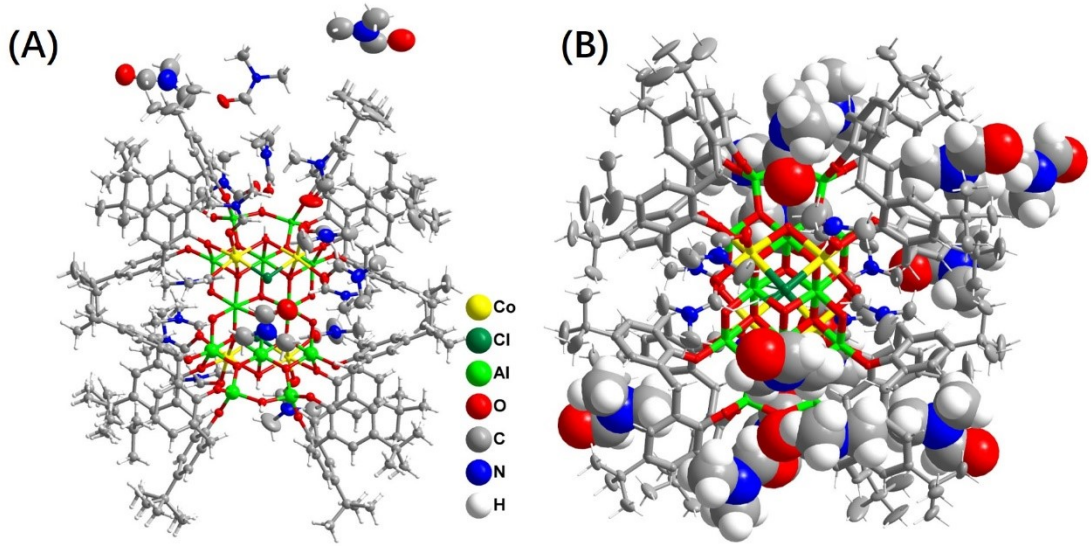

Figure S2. (A) and (B) The ORTEP-style view of $\mathbf{Al_{12}Co_4}$ cluster.

$\mathbf{Al_{12}Co_4}$ is isolated from the DMF. The molecular formula of $\mathbf{Al_{12}Co_4}$ was determined as $[Al_{12}Co_4O_8(OH)_{10}(TBC[4])_4(DMF)_8Cl_2]\cdot 18DMF$.

Some highly disordered solvent molecules in the crystal structures were removed with the SQUEEZE program in PLATON, and its possible formula was proposed based on the SQUEEZE and TGA results. SCXRD analysis showed the position of some guest DMF molecules.

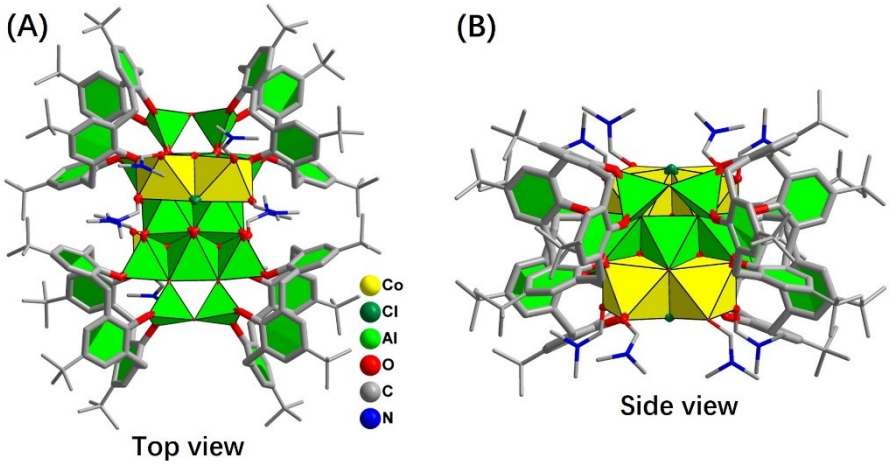

Figure S3. The polyhedral structure of the $\mathbf{Al_{12}Co_4}$ cluster, depicting both a top view (A) and a side view (B).

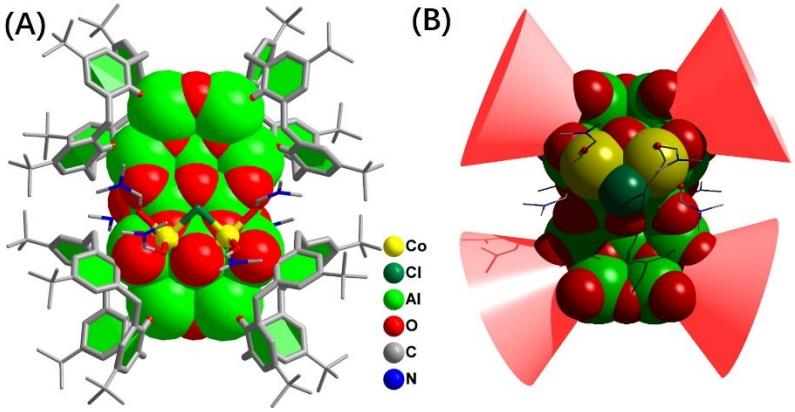

Figure S4. Topology structure of the $Al_{12}Co_4$ cluster.

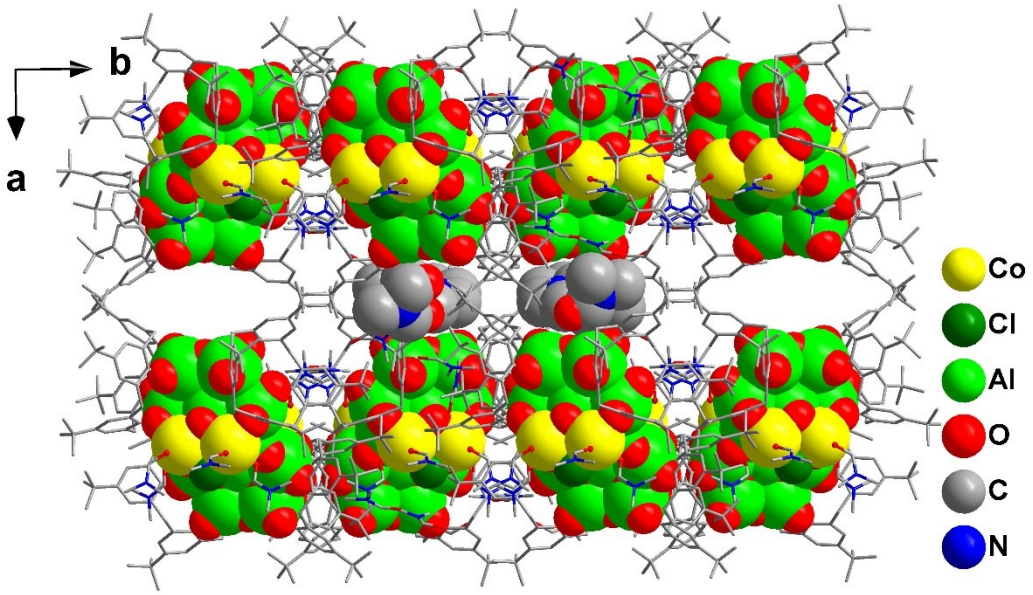

Figure S5. Packing structure of $Al_{12}Co_4$. highlighting the exposed Co ions on the surface.

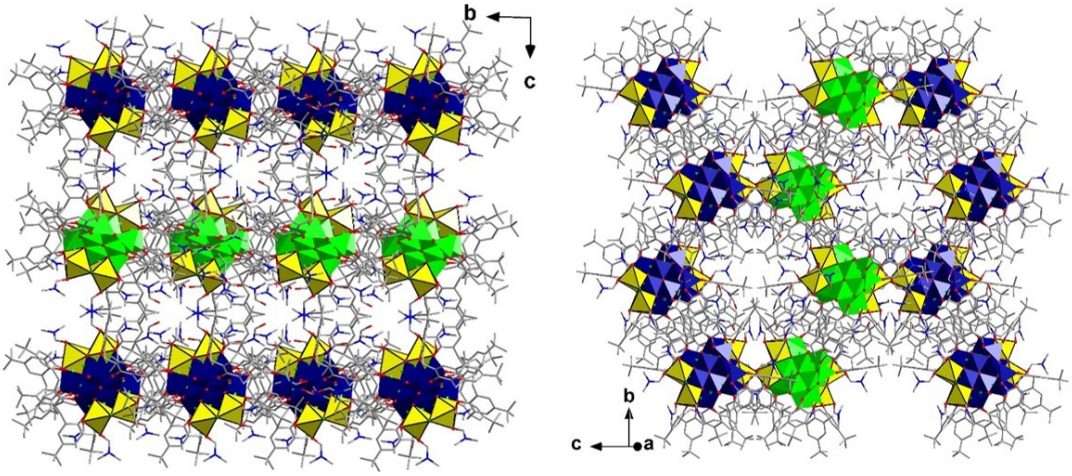

Figure S6. Three-dimensional packing structure of $Al_{12}Co_4$.

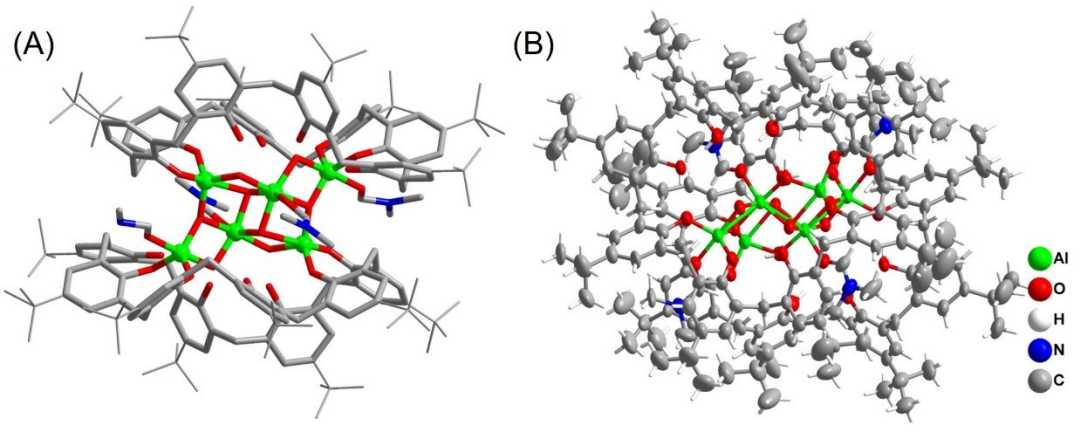

Figure S7. (A) and (B) Crystal structure of the Al_6 cluster.

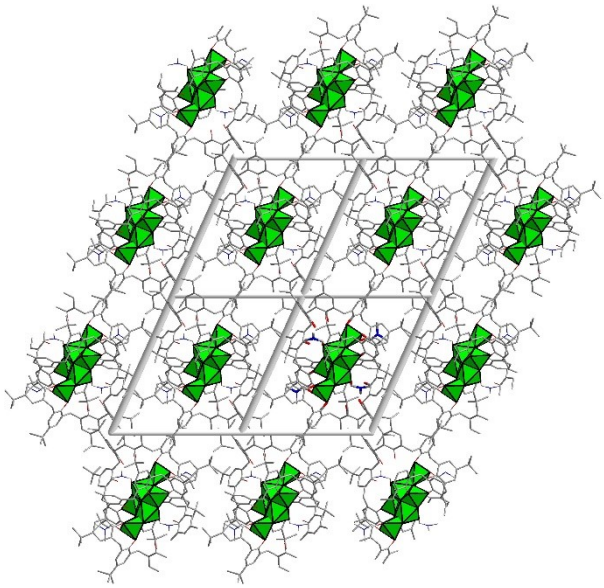

Figure S8. Three-dimensional packing structure of $\mathbf{Al_6}$ cluster.

2. Powder X-ray diffraction

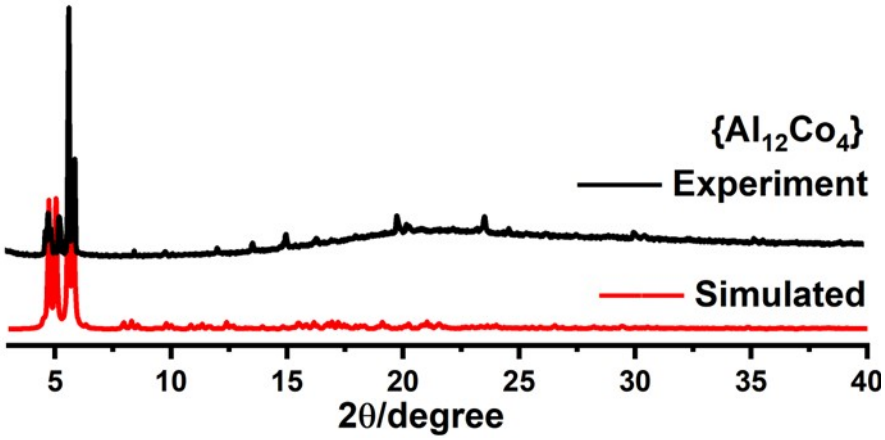

Figure S9. The XRD pattern of $\mathbf{Al_{12}Co_4}$ (the simulated pattern, as-synthesized product).

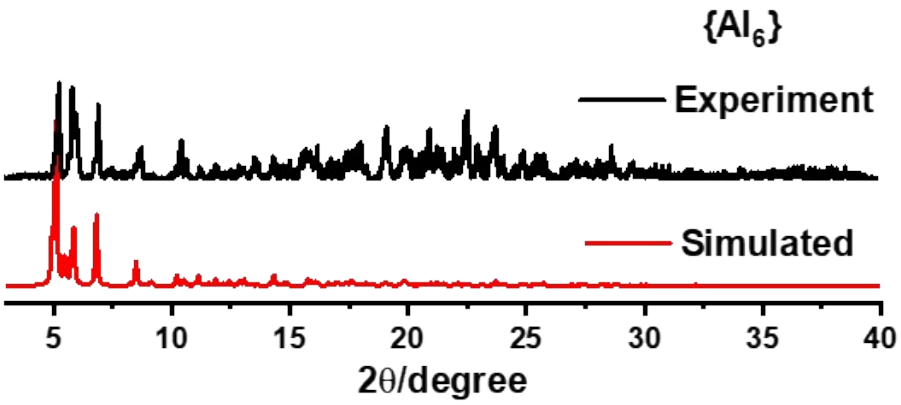

Figure S10. The XRD pattern of $\mathbf{Al_6}$ (the simulated pattern, as-synthesized product)

3. EDS patterns

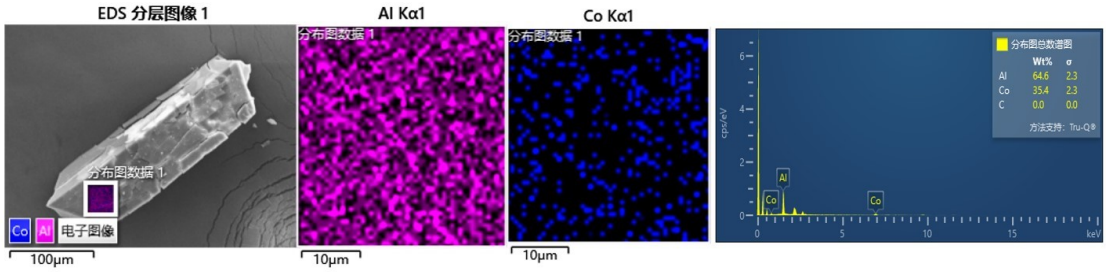

Figure S11. SEM and elemental mapping images of $Al_{12}Co_4$.

Table S2. ICP result of $Al_{12}Co_4$.

Element label	Weight (g)	Volume (ml)	Dilution coefficient	Instrument reading (mg/L)	Sample concentration(mg/kg)	Element ratio
Al	0.0245	25	100	0.864368680	88200.9	3.147731543
Co	0.0245	25	10	5.997836760	61202.4	

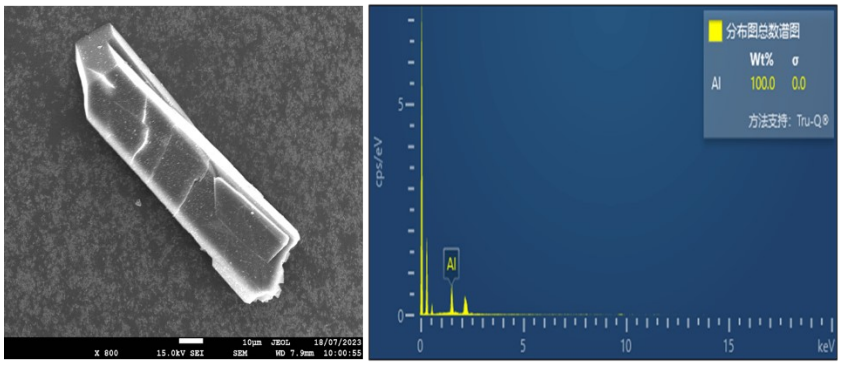

Figure S12. SEM and elemental mapping images of Al_6.

4. FT-IR spectrum

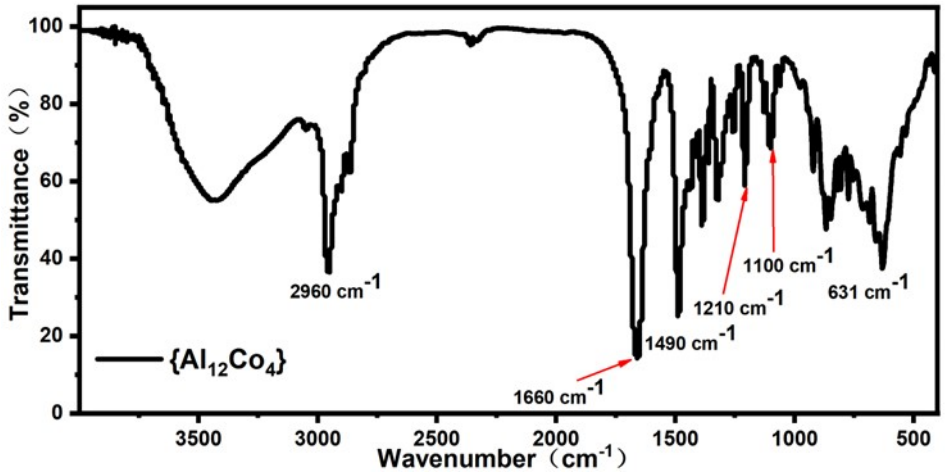

Figure S13. IR spectra of crystal samples of $Al_{12}Co_4$.

Discussion for IR spectra: The IR spectrum of $Al_{12}Co_4$ have been recorded in the range of 4000–400 cm^{-1} from solid samples palletized with KBr. In the high wavenumber region, the aboard

absorption bands from 3700 to 3200 cm^{-1} stem from the ν(O-H) stretching mode of -OH groups or water molecules. The bands at 3000−2800 cm^{-1} can be ascribed to the stretching vibration modes of C–H bonds in aromatic rings and tert butyl group. The strong vibration band at approximately 1660-1490 cm^{-1} can be attributed to the benzene ring skeleton vibration. The characteristic bands of Al-O and Co-O appears in the ranges of 500–750 cm^{-1}.

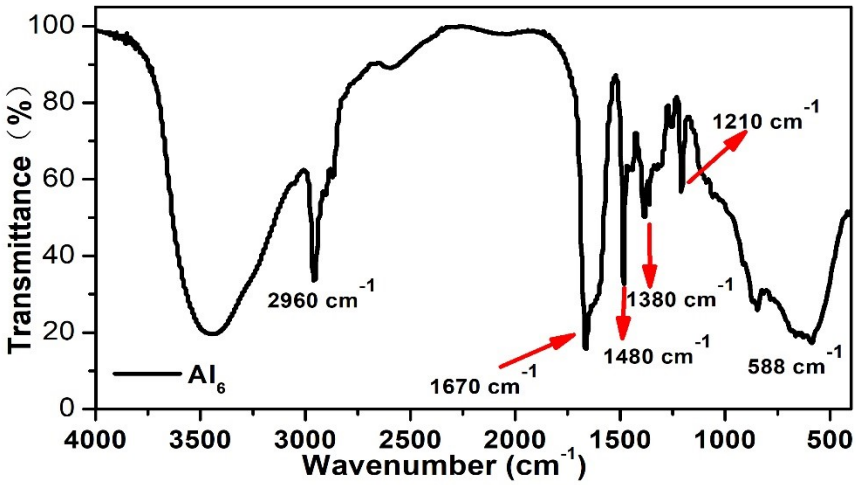

Figure S14. IR spectrum of crystal samples of $\mathbf{Al_6}$.

5. TG-Measurement.

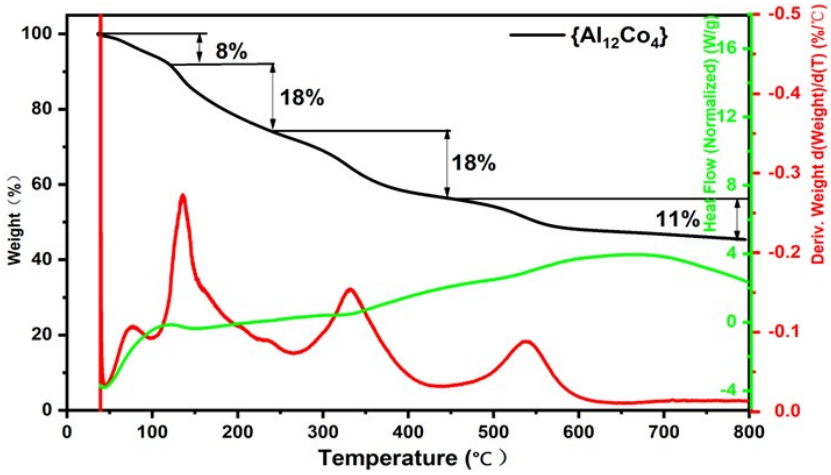

Figure S15. Thermal decomposition curve of the $\mathbf{Al_{12}Co_4}$ compound.

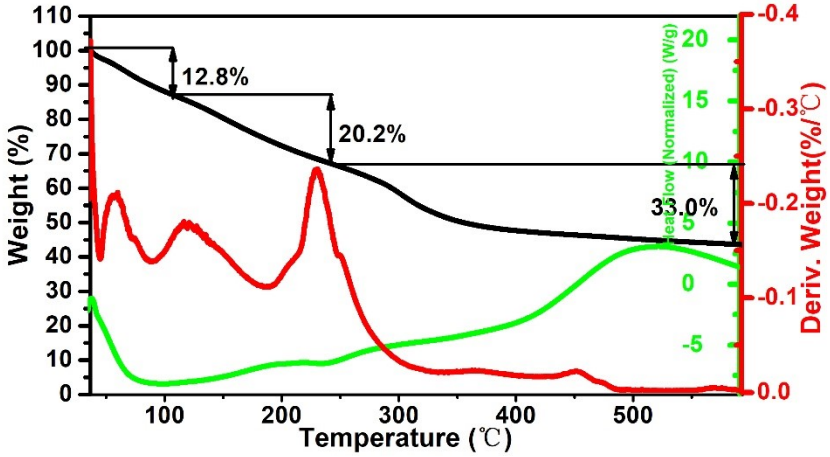

Figure S16. Thermal decomposition curve of the $\mathbf{Al_6}$ compound.

6. XPS Measurement.

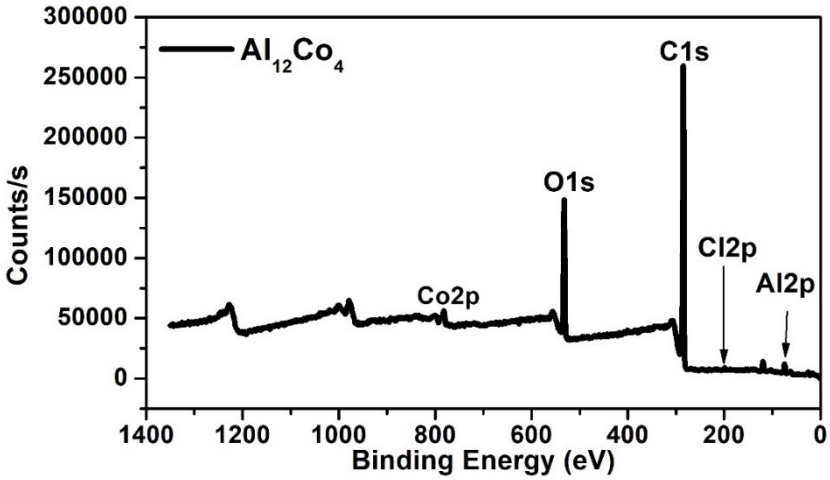

Figure S17. XPS survey spectrum of $\mathbf{Al_{12}Co_4}$ compound.

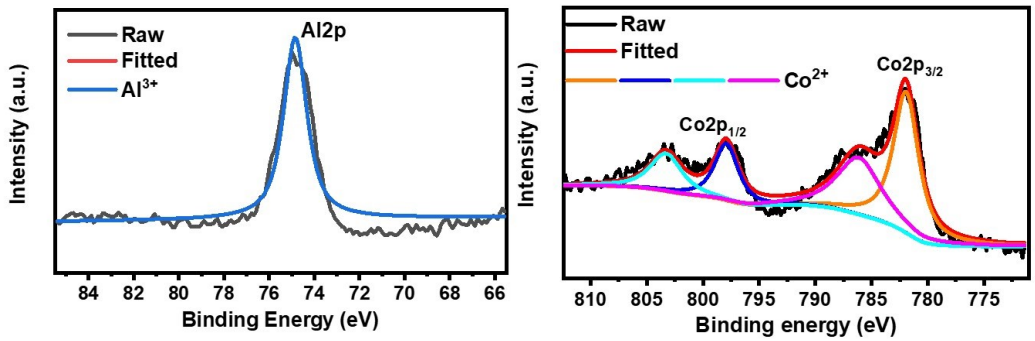

Figure S18. High resolution XPS spectra of (b) Al 2p, (c) Co 2p.

7. MALDI-TOF-MS Measurement.

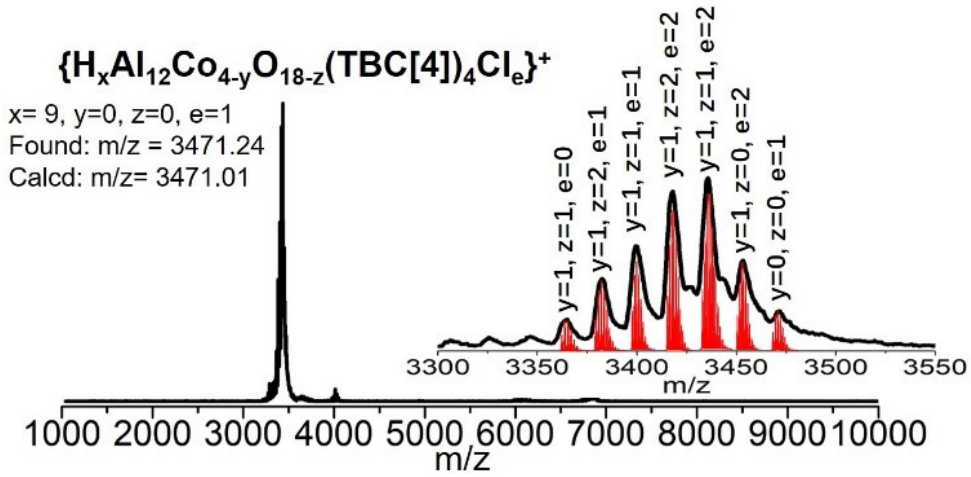

Figure S19. Positive-mode MALDI-TOF-MS spectrum of $\mathbf{Al_{12}Co_4}$ in chloroform solution.

8. Electrocatalytic performance.

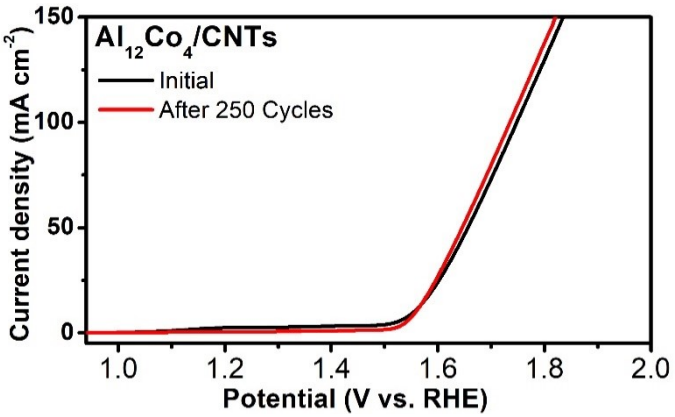

Figure S20. LSV curves of $\mathbf{Al_{12}Co_4}$/CNTs before and after 250 cycles test.

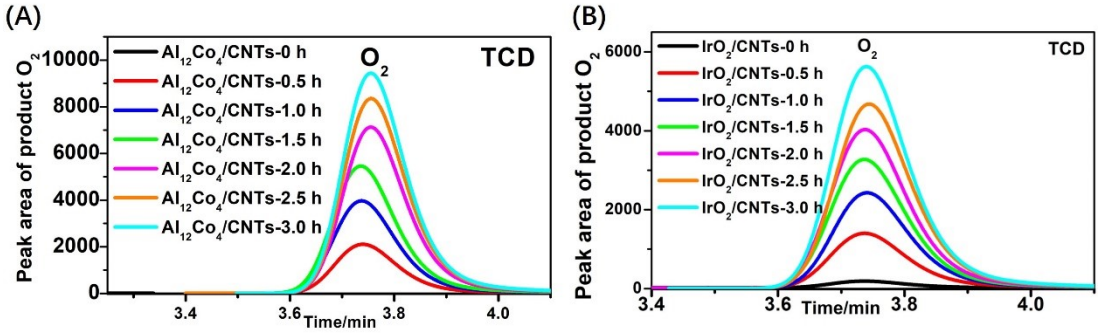

Figure S21. Gas chromatogram spectra of the O_2 product signal measured at a potential of 1.67 V (vs. RHE) for 3 h.

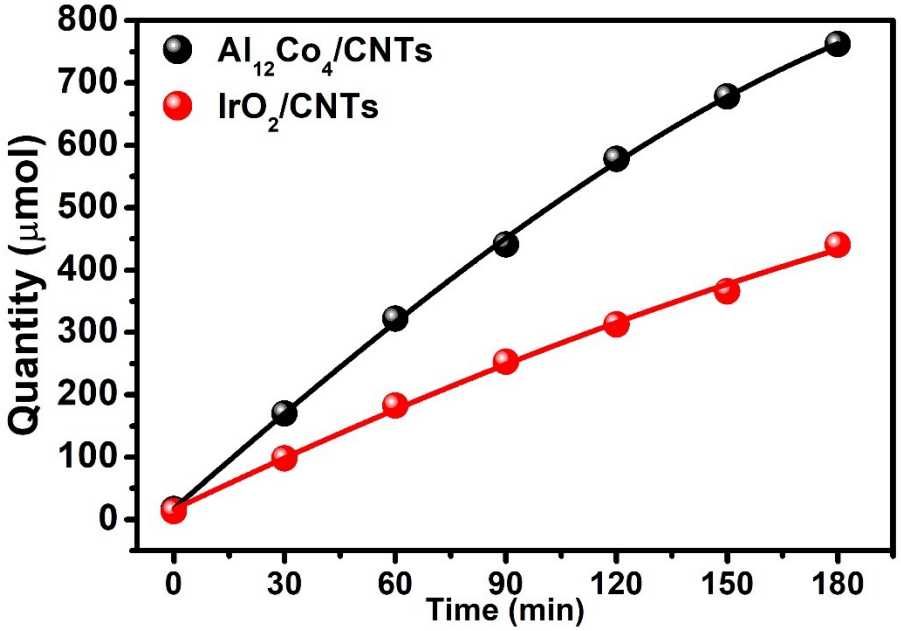

Figure S22. Electrocatalytic O_2 amount of **$Al_{12}Co_4$**/CNTs and IrO_2/CNTs.

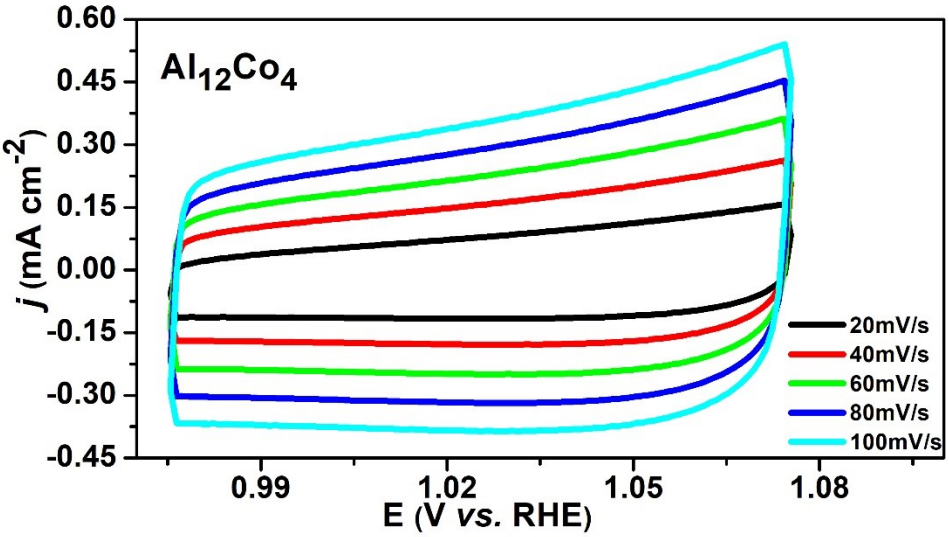

Figure S23. The cyclic voltammograms (CVs) measurements with various scan rates for **$Al_{12}Co_4$**/CNTs in 1.0 M KOH.

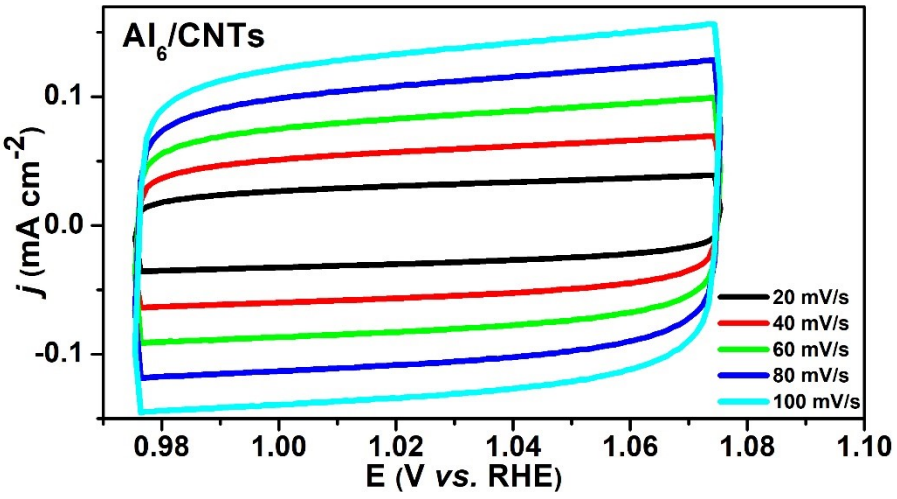

Figure S24. The cyclic voltammograms (CVs) measurements with various scan rates for **Al_6**/CNTs in 1.0 M KOH.

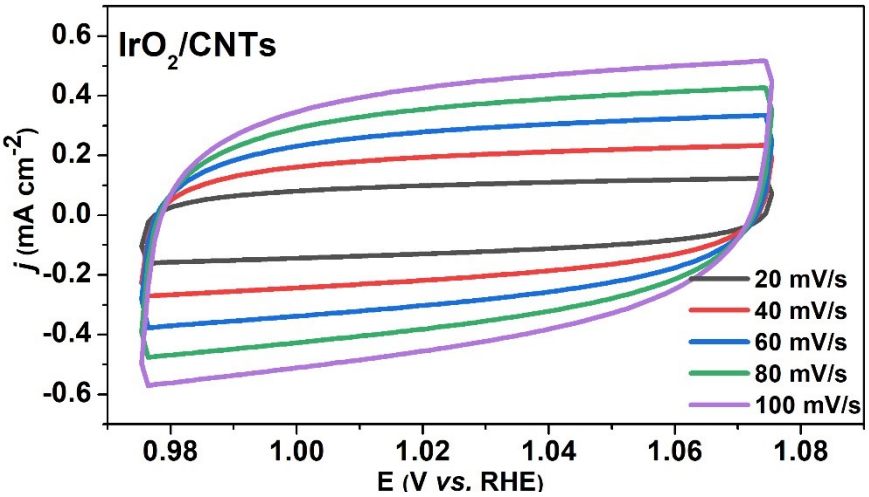

Figure S25. The cyclic voltammograms (CVs) measurements with various scan rates for **IrO_2**/CNTs in 1.0 M KOH.

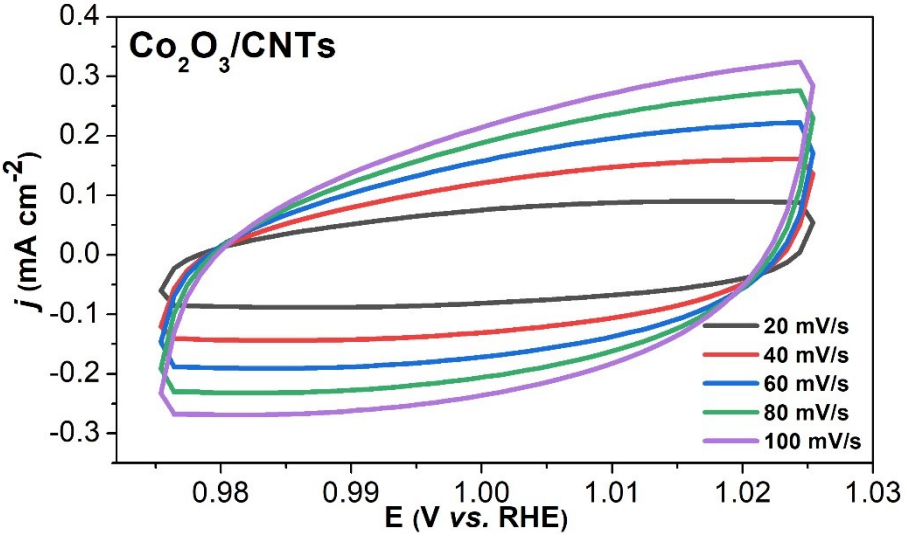

Figure S26. The cyclic voltammograms (CVs) measurements with various scan rates for **Co_2O_3**/CNTs in 1.0 M KOH.

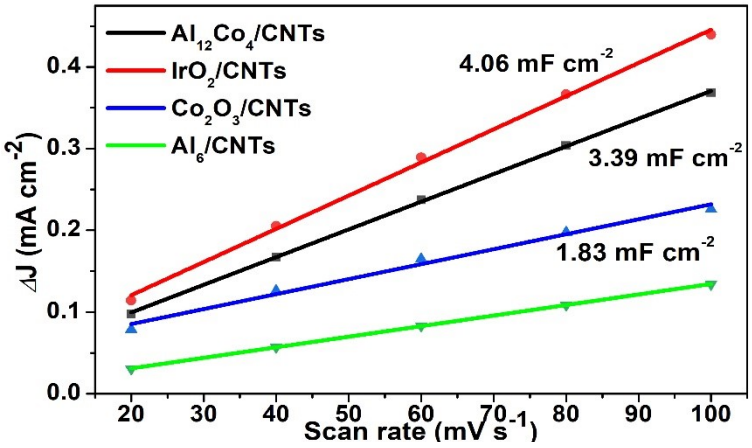

Figure S27. The capacitive current density ($J_{a/2}$-$J_{c/2}$) as a function of scan rate in the region of

0.97~1.03 V vs. RHE.

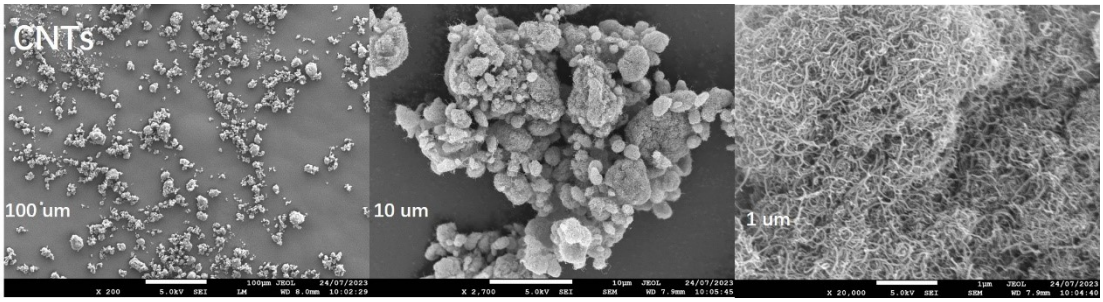

Figure S28. The SEM patterns of CNTs at different magnification: (a) 100 um, (b) 10 um, (c) 1 um.

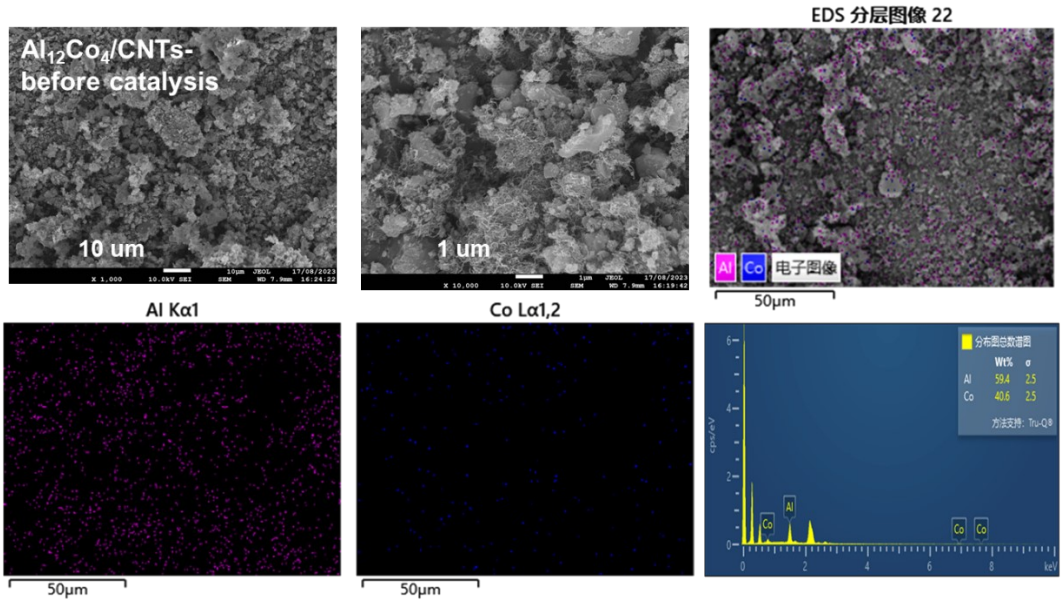

Figure S29. The EDS patterns of **$Al_{12}Co_4$**/CNTs before electrolysis.

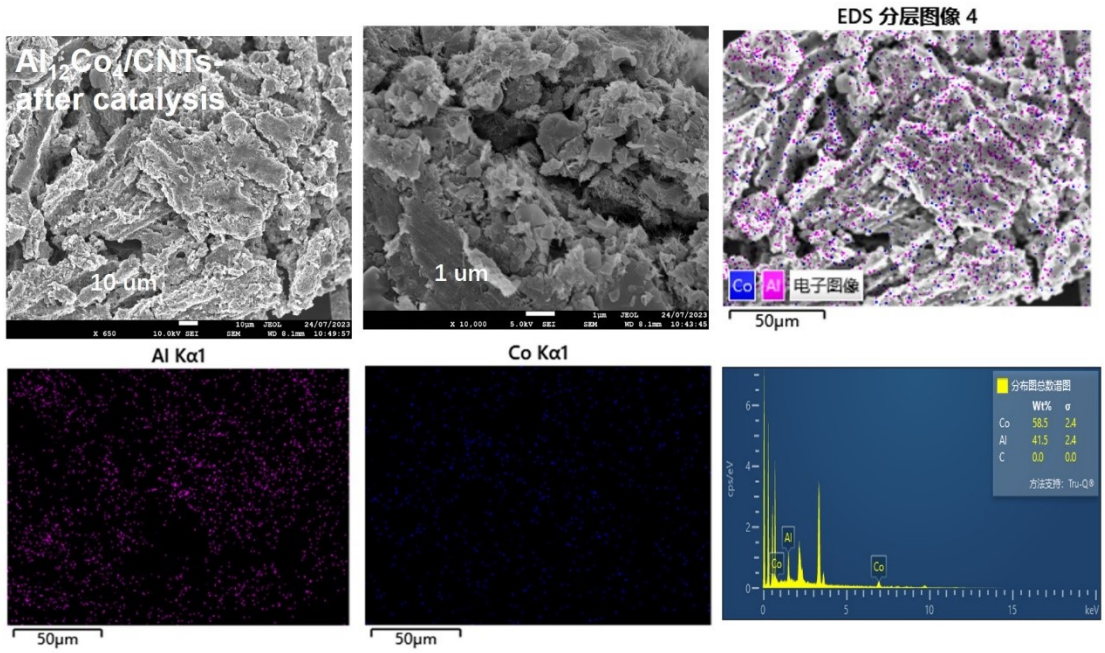

Figure S30. The SEM and EDS patterns of $Al_{12}Co_4$/CNTs-after electrolysis.

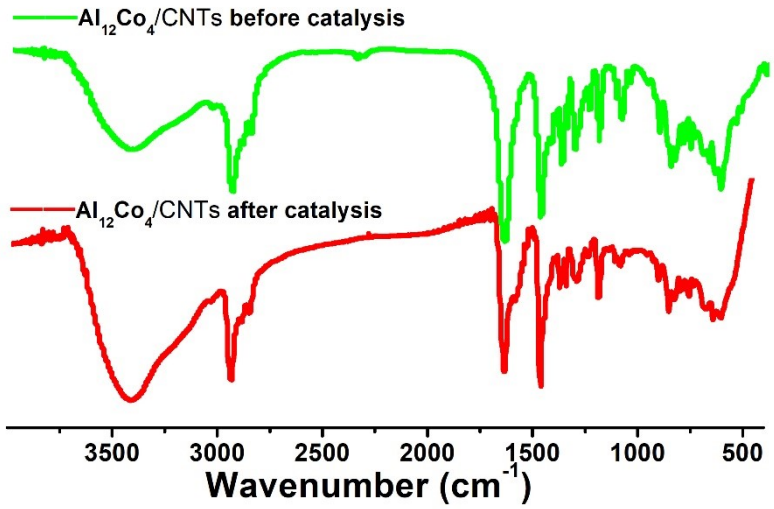

Figure S31. IR spectra of $Al_{12}Co_4$/CNTs before and after OER reaction.

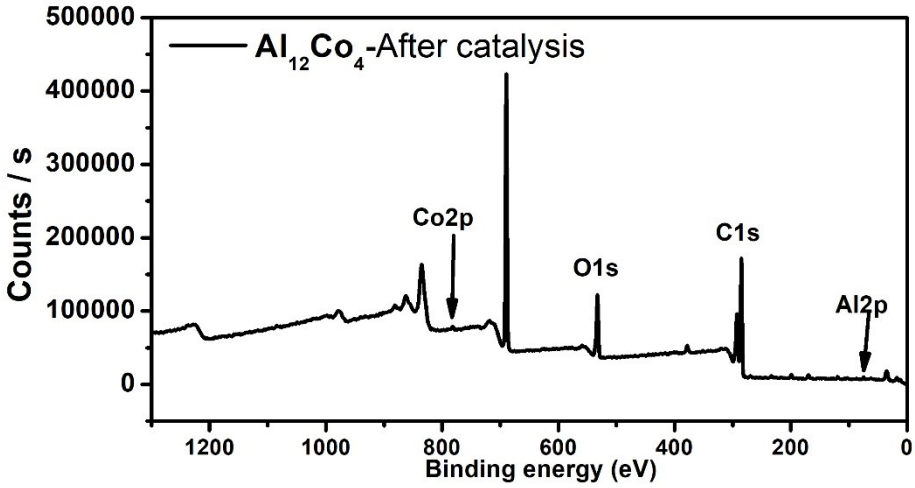

Figure S32. XPS survey spectrum of the catalyst after OER reaction.

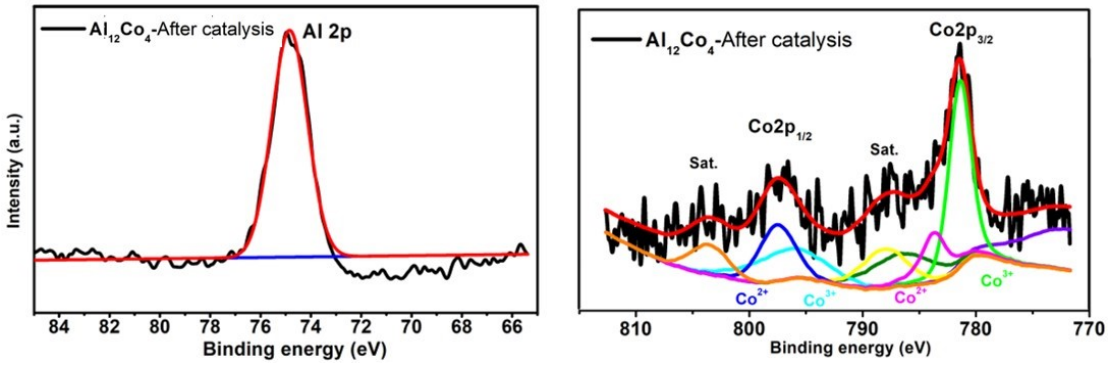

Figure S33. High-solution Al 2p and Co 2p XPS of the catalyst after OER reaction.

Table. S3 Comparison of electrocatalytic performances of Co-based materials for OER.

Catalyst	Substrate	Electrolyte	η_{10}	Reference
Co-BPDC/Co-BDC3	GCE	1 M KOH	335 mV	1

Co_4Mo_8	GCE	1 M KOH	424 mV	2
Co_4Mo_8	NF	1 M KOH	302 mV	2
Co-ZIF-9(III)	GCE	1 M KOH	380 mV	3
Unsaturated ZIF-67	GCE	1 M KOH	410 mV	4
CTGU-14	GCE	1 M KOH	454 mV	5
$Ti_{10}Co_2$	CC	1 M KOH	400 mV	6
$Al_{12}Co_4$/CNTs	CC	1 M KOH	**320** mV	**This work**

Reference:

1. Zha, Q.; Yuan, F.; Qin, G.; Ni, Y. Cobalt-based MOF-on-MOF two-dimensional heterojunction nanostructures for enhanced oxygen evolution reaction electrocatalytic activity. *Inorg. Chem*. **2020**, *59*, 1295–1305.
2. Zhang, M.; Chen, M. W.; Bi, Y. F.; Huang, L. L.; Zhou, K.; Zheng, Z. P. Bimetallic Co_4Mo_8 cluster built from Mo_8 oxothiomolybdate capped by Co_4-thiacalix[4]arene unit: the observation of Co-Mo synergistic effect for binder-free electrocatalyst. *J. Mater. Chem. A*. **2019**, *7*, 12893–12899.
3. Jiang, J.; Huang, L.; Liu, X.; Ai, L. Bioinspired cobalt-citrate metal-organic framework as an efficient electrocatalyst for water oxidation. *ACS Appl. Mater. Interfaces.* **2017**, *9*, 7193–7201.
4. Jayaramulu, K.; Masa, J.; Morales, D. M.; Tomanec, O.; Ranc, V.; Petr, M.; Wilde, P.; Chen, Y. T.; Zboril, R.; Schuhmann, W.; Fischer, R. A. Ultrathin 2D cobalt zeolite-imidazole framework nanosheets for electrocatalytic oxygen evolution. *Adv. Sci*. **2018**, *5*, 1801029.
5. Tao, L.; Lin, C. Y.; Dou, S.; Feng, S.; Chen, D.; Liu, D.; Huo, J.; Xia, Z.; Wang, S. Creating coordinatively unsaturated metal sites in metal-organic-frameworks as efficient electrocatalysts for the oxygen evolution reaction: Insights into the active centers. *Nano Energy*. **2017**, *41*, 417–425.
6. Tian, Y-Q.; Han, E-M.; Wan, B.; Yu, W-D.; Chen, M-Z.; Yan, J.; Yi, X.-Y.; Liu, C. Heterometallic Polyoxotitanium Cluster as Bifunctional Electrocatalyst for Overall Water Splitting, *Inorg. Chem*, 2022, **61**, 10151–10158.

9. BVS calculation.

Table S4. BVS calculation of the reported compounds.

$Al_{12}Co_4$

Atom	Atom	Length/Å	r0	lnS	S	valence state
Co1	Cl031	2.4717	2.01	-1.2478378	0.2871249	1.9596191
Co1	O00G	2.154	1.685	-1.2675675	0.2815155	
Co1	O00H	2.006	1.685	-0.8675675	0.4199718	
Co1	O00M	2.153	1.685	-1.2648648	0.2822774	
Co1	O00S	2.115	1.685	-1.1621621	0.3128091	
Co1	O00U	2.047	1.685	-0.9783783	0.3759202	
Co2	Cl03	2.4418	2.01	-1.1670270	0.3112910	1.9701222
Co2	O00A	1.999	1.685	-0.8486486	0.4279929	
Co2	O00J1	2.128	1.685	-1.1972972	0.3020093	
Co2	O00M1	2.208	1.685	-1.4135135	0.2432869	
Co2	O00R	2.146	1.685	-1.2459459	0.2876686	
Co2	O00T	2.026	1.685	-0.9216216	0.3978733	
Al1	O00A1	1.914	1.644	-0.7297297	0.4820392	3.0418714
Al1	O00B	1.797	1.644	-0.4135135	0.6613225	
Al1	O00C	1.777	1.644	-0.3594594	0.6980535	
Al1	O00E	1.843	1.644	-0.5378378	0.5840096	
Al1	O00J	1.823	1.644	-0.4837837	0.6164464	
Al6	O00A	1.823	1.644	-0.4837837	0.6164464	3.0904666
Al6	O00E1	1.897	1.644	-0.6837837	0.5047036	
Al6	O00H	1.827	1.644	-0.4945945	0.6098180	
Al6	O00K	1.957	1.644	-0.8459459	0.4291512	

Al6	O00K1	1.971	1.644	-0.8837837	0.4132164	
Al6	O00L	1.888	1.644	-0.6594594	0.5171307	
Al3	O00A1	1.894	1.644	-0.6756756	0.5088125	2.8358770
Al3	O00B	1.868	1.644	-0.6054054	0.5458530	
Al3	O00D	1.868	1.644	-0.6054054	0.5458530	
Al3	O00H	1.899	1.644	-0.6891891	0.5019829	
Al3	O00K1	2.213	1.644	-1.5378378	0.2148451	
Al3	O00M	1.887	1.644	-0.6567567	0.5185303	
Al4	O00D	1.742	1.644	-0.2648648	0.7673096	3.0386815
Al4	O00I	1.735	1.644	-0.2459459	0.78196449	
Al4	O00N	1.713	1.644	-0.1864864	0.8298697	
Al4	O00P	1.798	1.644	-0.4162162	0.6595376	
Al5	O00D	1.799	1.644	-0.4189189	0.6577575	3.0331782
Al5	O00F	1.772	1.644	-0.3459459	0.7075507	
Al5	O00G	1.835	1.644	-0.5162162	0.5967743	
Al5	O00H	1.915	1.644	-0.7324324	0.4807382	
Al5	O00L	1.839	1.644	-0.5270270	0.5903574	
Al2	O00B	1.738	1.644	-0.2540540	0.7756498	3.0125832
Al2	O00O	1.733	1.644	-0.24054054	0.7862027	
Al2	O00P	1.8	1.644	-0.4216216	0.6559822	
Al2	O00Q	1.729	1.644	-0.2297297	0.794748	